THE ASTROPHYSICAL JOURNAL, 417:351–367, 1993 November 1

EVOLUTION OF THE SOLAR NEBULA. II. THERMAL STRUCTURE DURING NEBULA FORMATION

ALAN P. BOSS
Department of Terrestrial Magnetism, Carnegie Institution of Washington, 5241 Broad Branch Road, NW, Washington, DC 20015-1305
Received 1992 December 31; accepted 1993 May 10

ABSTRACT

Models of the thermal structure of protoplanetary disks are required for understanding the physics and chemistry of the earliest phases of planet formation. Numerical hydrodynamical models of the protostellar collapse phase have not been evolved far enough in time to be relevant to planet formation, i.e., to a relatively low-mass disk surrounding a protostar. One simplification is to *assume* a pre-existing solar-mass protostar, and calculate the structure of just the disk as it forms from the highest angular momentum vestiges of the placental cloud core. A spatially second-order accurate, axisymmetric (two-dimensional), radiative hydrodynamics code has been used to construct three sets of protoplanetary disk models under this assumption. Because compressional heating has been included, but not viscous or other heating sources, the model temperatures obtained should be considered lower bounds. The first set started from a spherically symmetric configuration appropriate for freely falling gas: $\rho \propto r^{-3/2}$, $v_r \propto r^{-1/2}$, but with rotation ($\Omega \propto r^{-1}$, where r is the spherical coordinate radius). These first models turned out to be unsatisfactory because in order to achieve an acceptable mass accretion rate onto the protostar ($\dot{M}_s \leq 10^{-5}\ M_\odot\ \mathrm{yr}^{-1}$ for low-mass star formation), the disk mass became much too small ($\sim 0.0002\ M_\odot$). The second set improved on the first set by ensuring that the late-arriving, high angular momentum gas did not accrete directly onto the protosun. By starting from a disk-like cloud flattened about the equatorial plane and flowing vertically toward the midplane, these models led to $\dot{M}_s \rightarrow 0$, as desired. However, because the initial cloud was not chosen to be close to equilibrium, the disk rapidly contracted vertically, producing an effective *disk* mass accretion rate $\dot{M}_d \sim 10^{-2}\ M_\odot\ \mathrm{yr}^{-1}$, again too high. Hence, the third (and most realistic) set started from an approximate equilibrium state for an adiabatic, self-gravitating "fat" Keplerian disk, with surface density $\sigma \propto r^{-1/2}$, surrounded by a much lower density "halo" infalling onto the disk. This initial condition produced $\dot{M}_s \rightarrow 0$ and $\dot{M}_d \sim 10^{-6}$ to $10^{-5}\ M_\odot\ \mathrm{yr}^{-1}$, as desired. The resulting nebula temperature distributions show that midplane temperatures of at least 1000 K inside 2.5 AU, falling to around 100 K outside 5 AU, are to be expected during the formation phase of a minimum mass nebula containing $\sim 0.02\ M_\odot$ within 10 AU. This steady state temperature distribution appears to be consistent with cosmochemical evidence which has been interpreted as implying a phase of relatively high temperatures in the inner nebula. The temperature distribution also implies that the nebula would be cool enough outside 5 AU to allow ices to accumulate into planetesimals even at this relatively early phase of nebula evolution.

Subject headings: accretion, accretion disks — hydrodynamics — solar system: formation

1. INTRODUCTION

One perplexing discrepancy in our understanding of solar system formation has been between meteoritical evidence for high temperature processing of pre-asteroidal materials on the one hand, and standard viscous accretion disk models of protoplanetary disks with much lower (~ 150 K) midplane temperatures at 2 to 3 AU (Wood & Morfill 1988). The low volatile metal contents measured for chondritic meteorites and inferred for the terrestrial planets have been interpreted as requiring a prolonged period of chemical fractionation caused by depletion of volatile metal-rich nebular gas at temperatures in the range 1200 to 1400 K (Palme & Boynton 1992). Widespread variations in Mg and Si abundances among chondrites have been interpreted as implying similar temperatures in order to evaporate portions of olivine grains (Larimer & Wasson 1988; Palme & Boynton 1992). Both of these compositional trends may be explained by a nebular phase with midplane temperatures around 1300 K. In addition, chondrules and certain refractory inclusions evidently experienced even higher (~ 1500 to ~ 2000 K) temperatures, but because chondrule textures and compositions also require rapid ($\sim$ hours) heating and cooling (Hewins 1988), the formation of chondrules appears to require a series of localized heating events largely unrelated to the midplane temperature profile (Wood 1988; Hood & Horanyi 1991; Boss & Graham 1993). Localized heating events might also be capable of explaining the volatile metal abundances in regions of the nebula with considerably lower temperatures than 1300 K (e.g., well above the nebula midplane). In order to advance our incomplete understanding of meteorite parent body and planetesimal formation, detailed models of the radial and vertical temperature distribution in the solar nebula are required.

Nebula temperatures are also important for determining the location of the ice condensation point, outside of which the surface density of solids will increase significantly. The surface density of solid matter is a key determinant of how rapidly the planetary formation process proceeds through the collisional accumulation of planetesimals (Wetherill 1990). The location of the ice condensation point is also crucial to the Stevenson & Lunine (1988) suggestion that giant planet formation might result from an enhancement of icy matter produced by turbulent transport of water vapor from the inner nebula outward to

the condensation point. Temperatures in the outer nebula must also be reconciled with the observed volatile abundances in comets, which require that comets formed at about 60 K or even lower temperatures (Mumma, Weissman, & Stern 1992).

Standard viscous accretion disk theory (e.g., Pringle 1981) assumes the existence of a low-mass (non–self-gravitating), thin disk in Keplerian rotation about a mass point, approximations that are commonly used in modeling the solar nebula. Disk evolution is further assumed to be dominated by viscous shear, with the viscosity being characterized by a free parameter α, and with viscous dissipation being the primary source of disk heating. The vertical thermal profile can then be approximated once the vertical optical depth of the disk is specified.

Ruden & Lin (1986) presented time-evolving models of viscous accretion disks, starting with midplane temperatures of about 1000 K out to 10 AU, but dropping to values around 300 K at 2 AU within about 4×10^5 yr. Cabot et al. (1987) found midplane temperatures to be on the order of 300 K at 2 AU in their steady state, viscous accretion disk models. Ruden & Pollack (1991) found midplane temperatures of $\sim$1000 K at 2 AU to 3 AU, but only during the initial, dynamic phase of their calculations, when the disk mass was greater than $\sim 0.1\ M_\odot$ and mass was being transported inward to the protosun; their final, steady state temperatures at 2 AU to 3 AU were $\sim$10 K.

If a viscous accretion disk is to have a midplane temperature of 1500 K at 3 AU and a mass accretion rate $\dot{M} \sim 10^{-6}\ M_\odot\ \mathrm{yr}^{-1}$, then the viscosity parameter $\alpha \sim 10^{-6}$ (Morfill 1988), and so the disk mass (out to 50 AU) must be $\sim 0.5\ M_\odot$, using the disk mass relation of Wood & Morfill (1988). Such a massive disk around a solar-mass protostar would violate the basic assumption of a low-mass disk, and would not be applicable to planetary formation processes because most of this disk mass presumably would end up in the protostar. Estimates of the "minimum mass" needed to account for formation of the solar system's planets are about a factor of 10 lower -0.01 to $0.07\ M_\odot$ (Weidenschilling 1977).

Viscous accretion disk models generally derive their luminosity solely from viscous dissipation associated with the transport of nebula mass inward to the central protostar, and so neglect any energy derived from matter infalling onto the nebula from the parent molecular cloud core. Cassen & Moosman (1981) and Cassen & Summers (1983), however, did include the effects of infalling gas on ballistic trajectories in their viscous accretion disk models, finding surface temperatures of $\sim$100 K at a few AU in minimum mass disks (midplane temperatures were not calculated but "might be several times hotter," Cassen & Summers 1983). Ruzmaikina & Maeva (1986) also included accretion of gas onto the disk, and found midplane temperatures of $\sim$300 K at 2 to 4 AU in a viscous accretion disk with a final mass of $0.1\ M_\odot$. Lin & Pringle (1990) calculated viscous accretion disks forming through infall, assuming that all of the available kinetic energy of the infalling matter went into heating the disk, but limited their models to radii greater than 13 AU.

A parallel effort to the work on viscous accretion disks over the last two decades has been the development of fully numerical solutions of the multidimensional equations of hydrodynamics. Numerical solutions can be attempted without having to employ the approximations often necessary for an analytical or semi-analytical solution (e.g., idealized symmetry, simplified thermodynamics, vertically thin disks, no self-gravitation). Numerical models of solar nebula formation may either ignore the effects of turbulence and viscous dissipation (e.g., Boss 1989; Bodenheimer et al. 1990) or include the effects of an α-viscosity (e.g., Tscharnuter 1987), but all include compressional heating from the collapsing gas and radiative transfer in either the diffusion or Eddington approximation.

Numerical three-dimensional hydrodynamical models of nebula formation produced high ($\sim$1500 K) midplane temperatures at 2 to 3 AU (Boss 1988, 1989) even in a minimum mass nebula, but the models effectively had high mass accretion rates ($\dot{M} \sim 10^{-3}$ to $10^{-2}\ M_\odot\ \mathrm{yr}^{-1}$), well above the generally accepted range of $\dot{M} \sim 10^{-6}$ to $10^{-4}\ M_\odot\ \mathrm{yr}^{-1}$ for low-mass protostars. Numerical two-dimensional hydrodynamical models found similarly high temperatures in the inner nebula for comparable or slightly smaller mass accretion rates (Tscharnuter 1987; Bodenheimer et al. 1990), but in these models the final nebula masses ($>0.4\ M_\odot$) were considerably higher than the minimum mass nebula, so these models cannot be applied to later phases when planetary accumulation was beginning. Tomley, Cassen, & Steiman-Cameron (1991) used a two-dimensional planar N-body code to model the interaction between gravitational instabilities and an imposed disk cooling law, but their disk models were restricted to radii within 41 stellar radii (<1 AU).

Other calculations of nebula properties do not fit as easily into the viscous accretion disk or numerical hydrodynamics framework. Terebey, Shu, & Cassen (1984) and Stemwedel, Yuan, & Cassen (1990) used semi-analytical techniques to study the collapse of rotating clouds, assuming isothermality and zero gas pressure, respectively, and so neither study addressed the question of nebula temperatures. Note that the zero pressure assumption used by Stemwedel et al. (1990) means that their disks retain no internal energy from the collapsing gas, which is the opposite of the assumption made by Lin & Pringle (1990). Wood (1984) calculated the shock heating expected at the nebula accretion shock, based on a simple model of cloud infall and an estimate of the nebula photospheric temperature, but did not attempt to calculate midplane temperatures. Watanabe, Nakagawa, & Nakazawa (1990) studied the question of convective stability during the quasi-static contraction of a vertical segment of a minimum mass nebula at 1 AU. Watanabe et al. (1990) found that convection was rapidly stabilized by solar heating at the nebula surface. Their models started with midplane temperatures of 1000 K and quickly cooled to $\sim$500 K at 1 AU. Cassen (1992) used observations of the radial variation of the photospheric temperature inferred for T Tauri disks to construct theoretical models of the temperature distribution in optically thick disks. Cassen (1992) found midplane temperatures of $\sim$1500 K out to about 3 AU, falling to values of $\sim$100 K around 30 AU.

Given these prior results, a few preliminary conclusions may be drawn. Viscous accretion disk models apparently lead to temperatures of only $\sim$300 K at 2 AU to 3 AU in a minimum mass nebula; the higher temperatures seemingly required by the cosmochemical evidence only occur in more massive viscous accretion disks. The assumptions that are usually necessary for making viscous accretion disk models tractable (e.g., neglect of compressional heating and self-gravity, and the approximate treatment of vertical radiative losses) are such as to suggest that different results might be obtained if some of these important assumptions could be relaxed. In principle, definitive calculations could be performed with numerical hydrodynamics codes, but the models constructed to date either have had mass accretion rates that are probably too high

for low-mass protostar formation, were not evolved far enough in time to be applicable to planetary formation, or both.

The purpose of this paper is to attempt to overcome both of these major problems through a new sequence of numerical hydrodynamical calculations. Assuming the prior existence of a solar-mass protostar, these models follow the collapse of the remaining molecular cloud core material onto the protoplanetary disk. Three different sets of numerical models have been investigated, with increasing degrees of refinement, and these are described in sequence in the following sections. We shall see that through a suitable choice of initial conditions, solar nebula models can be constructed that meet the twin criteria of having low mass accretion rates and low disk masses appropriate for a minimum mass nebula. The extent to which the resulting disk temperature distributions agree with the cosmochemical evidence is discussed in the final section.

It is important to note that the present modeling effort results in a prediction for nebula temperatures that depends solely on a small number of widely accepted parameters: a low-mass nebula, a solar-mass protosun, and mass accretion by the nebula at an astronomically inferred rate. The extent to which the results then agree with any particular meteoritical interpretation is of great interest, but it must be emphasized that the meteoritical interpretations have not been used to constrain or construct the models in any way.

NUMERICAL METHODS

2.1. *Equations and Numerical Grid*

An improved multidimensional radiative hydrodynamics code has been used to calculate the three sets of models presented in this paper. The code is described in detail elsewhere (Boss & Myhill 1992) and so only a brief description is given here. The explicit, Eulerian numerical code has been shown by convergence testing to be spatially second-order accurate. Advective fluxes are based on van Leer monotonic interpolation and consistent advection, as generalized to a spherical coordinate grid. The radial advective terms have been corrected for the volume-centering effect in spherical geometry. A tensor artificial viscosity is included, designed to vanish during homologous collapse (Tscharnuter & Winkler 1979). Self-gravity is included through a spherical harmonic expansion of the Poisson equation. Radiative transfer is included through an alternating directions implicit solution of the mean intensity equation in the Eddington approximation. Global conservation of mass, angular momentum, and internal energy are achieved through solving the hydrodynamical equations in conservation law form. Local conservation of angular momentum has been optimized by choosing a method for advecting angular momentum that best preserves the specific angular momentum spectrum during axisymmetric collapse.

Compressional heating associated with collapsing or contracting gas is the primary source of energy in the models—viscous and magnetic heating are neglected, and heating due to artificial viscosity is not important in most models. Hence the models should yield a lower bound on nebula temperatures, given that turbulence or ohmic dissipation could be occurring in portions of the nebula. The models are tested for convective instability (Schwarzschild 1965) in the r and θ directions, in order to learn if convectively driven turbulence should be occurring.

In order to minimize the computational burden while focusing on thermodynamics, all of the new models assume symmetry about the rotation axis (and about the midplane) and so are two-dimensional in space. The calculational grid extends from about 1 AU outward to either 10, 25, or 50 AU, with uniform radial grid spacings $\Delta r = 0.18$, 0.5, or 1 AU, respectively ($N_r = 51$). The θ grid is nonuniform ($\Delta\theta_j = 1.2\,\Delta\theta_{j-1}$) in order to enhance the vertical spatial resolution in the disk ($N_\theta = 23$ grid points for $\pi/2 \geq \theta \geq 0$); the minimum θ spacing of $\Delta\theta = 0.^\circ 3$ occurs at the midplane. Constant volume boundary conditions are imposed at the spherical outer boundary.

2.2. *Sink Cell*

In order to try to simulate solar nebula formation without including all of the details of protosun evolution, the calculations use a central "sink cell" (Boss & Black 1982) with an initial mass of 1 $M_\odot$ to represent the protosun's gravity and luminosity. The central protostar luminosity L_s is calculated from

$$L_s = \frac{GM_s\dot{M}_s}{R_s}, \tag{1}$$

where G is the gravitational constant, M_s is the protostar mass, $\dot{M}_s$ is the protostar mass accretion rate, and R_s is the protostar radius. This equation was used previously by Bodenheimer et al. (1990), and is known from radiative hydrodynamical calculations to be an accurate approximation (e.g., Winkler & Newman 1980). The protostellar radius was taken to be 3.5 $R_\odot$, as is appropriate for young protostellar cores (Stahler, Shu, & Taam 1980b).

The protostellar luminosity heats the central cell, and hence affects the disk temperature through the central temperature. For models where the instantaneous mass accretion rate is higher than generally accepted, the protostellar luminosity would be proportionately higher than is reasonable, leading to overly high central temperatures. Hence, the central temperature was not allowed to exceed either 1500 or 1700 K, so that even in cases where $\dot{M}_s$ is apparently too high, the disk temperatures would not necessarily also be unrealistically high. A temperature of $\sim$1700 K at or inside about 1 AU is consistent with the results of spherically symmetrical (one-dimensional) models of the formation of a solar-mass protostar (Tscharnuter & Winkler 1979, see their Figs. 1 and 2), and with the spectral energy distribution models of Adams & Shu (1985) for solar-mass protostars accreting at $10^{-5}\ M_\odot\ \mathrm{yr}^{-1}$.

The hydrodynamical fluxes between the central sink cell and the first radial shell of cells are altered to allow flow into, but not out of, the central cell. The gravitational potential due to the mass in the spherical central cell is added separately into the potential obtained from the solution of the Poisson equation for the disk material. In the last set of models, infall velocities are limited to being less than 42 km s^{-1} (the free fall velocity at 1 AU for $M_s = 1\ M_\odot$), in order to enhance numerical stability, and v_θ is required to be positive (i.e., directed toward the disk midplane).

2.3. *Radiative Transfer*

The Eddington approximation f factor, which enters into the mean intensity equation, was chosen to be either $\frac{1}{3}$ or 1. The former value is appropriate for early phases of collapse, when the radiation field is fairly isotropic, while the latter value is appropriate at later phases when the presence of a solar-mass protostar results in a radiation field that is mostly directed outward (Tscharnuter & Winkler 1979). In practice, though,

the choice of f was found to have little effect on the nebula temperature distributions.

The critical optical depth τ_c, used to decide which form for the radiative flux should be used (see eq. [5] of Boss & Myhill 1992), was set equal to 10 for most models. For comparison, the optical depth along a ray through the disk midplane to the central cell was over 10^4 for the third set of models, whereas the optical depth along the rotational axis (where very low densities occur) was $\sim 10^{-1}$.

The boundary condition on the mean intensity J was varied to discern its effects on the temperature distributions. This boundary condition was found to have little or no effect on the temperatures in the inner nebula, but to have an effect on the temperatures near the calculational boundary. In previous collapse calculations, the choice of this boundary condition has not been a problem, because the outer boundary is well-removed from the region of interest, and as long as the boundary conditions lead to $T = 10$ K, the temperature distribution is reasonably accurate. However, in order to have high spatial resolution in the radial direction, the outer boundary in the present models is uncomfortably close (i.e., at 10 or 25 AU) to the regions of most interest, e.g., 5 AU. Hence there is a need for a well-chosen boundary condition on J.

The boundary condition employed by Boss (1984) was

$$J_R = B_R + \frac{L}{4\pi R_R^2}, \tag{2}$$

where B is the Planck function, L is the total luminosity, and R_R is the radius of the spherical boundary. Equation (2) is appropriate for a cloud with roughly spherically symmetric emission and with a radius R_R well outside the emitting regions, and this boundary condition was used in some of the models. However, equation (2) is not necessarily appropriate for the present models, because protoplanetary disks can be expected to emit with different intensities when viewed edge-on or pole-on, and $R_R = 10$ or 25 AU is still within the emitting region of the disk. Adams & Shu (1986) used a "radiative zero" boundary condition, i.e., $J = 0$ as $r \rightarrow \infty$, which is not useful here either. Setting $J_R = B_R = \sigma T_R^4/\pi$ with $T_R = 10$ K would simply lead to a lower bound on temperatures in the outer nebula. Tscharnuter (1987), following Yorke (1980), used a variant of the following boundary condition

$$J_R = B_R + \frac{1}{3\kappa\rho}\left(-\frac{\partial J}{\partial r}\right), \tag{3}$$

where κ is the opacity and ρ is the density. Equation (3) is similar to equation (2), but has the advantage of being a local criterion which is not dependent on the total luminosity. With equation (3), J_R can vary from the pole to the equator, and thereby allow the outer regions of the disk to be cooler than the rarefied gas along the rotational axis, which is unshielded from the central protostar luminosity. Hence equation (3) was used in most of the models, but implemented in the form suggested by Tscharnuter (1987)

$$J_R = B_R + \frac{\delta J}{1 + \kappa\rho\,\Delta r}, \tag{4}$$

where $\delta J = J_{N_r-1} - J_{N_r}$ and $\Delta r = r_{N_r} - r_{N_r-1}$, in order to maintain stability for the small optical depths that occur near the rotation axis.

2.4. *Time Step*

Because of the explicit solution of the hydrodynamical equations (specifically the energy equation), numerical stability places the following constraint on the time step Δt

$$\Delta t < \left(\frac{\tau^2 E}{\kappa\sigma T^4}\right) \sim 10^4 s \left(\frac{\tau}{1}\right)^2 \left(\frac{T}{1000\ \mathrm{K}}\right)^{-3}, \tag{5}$$

where τ is the (gray) optical depth, E is the specific internal energy, σ is the Stefan-Boltzmann constant, and T is the temperature. Because of the occurrence of low optical depths and relatively high temperatures in the models, the resulting small size of the time step restricts the amount of elapsed time in the calculations to the order of years, even for calculations lasting $\sim 10^5$–10^6 time steps and using over a week of CPU time on an HP/Apollo DN-10040 workstation. Clearly this explicit time step constraint must be lifted before three-dimensional models become practical, which will require development of an implicit solution scheme for the three-dimensional energy equation. Bodenheimer et al. 1990 used an implicit solution for a portion of the two-dimensional energy equation in order to avoid this time step restraint.

This limitation to time evolutions on the order of years means that the present numerical models will not be able to follow the entire process of formation of the nebula, even in the restricted problem we have defined here, i.e., assuming the prior formation of a solar-mass protostar. If a low-mass disk ($\sim 10^{-2}\ M_\odot$) is to build up through accretion at $\dot{M} \sim 10^{-5}\ M_\odot\ \mathrm{yr}^{-1}$, then $\sim 10^3$ yr of evolution would be required. Hence most of the models will only be able to accomplish a task more limited than that which hydrodynamical codes usually perform, namely, searching for a steady state temperature distribution that applies to an initial assumed density and velocity distribution for the disk. To the extent that the initial density and velocity distribution changes during the course of the calculation, of course, a fully self-consistent solution for the problem will result, given that the usual equations of hydrodynamics are still being solved. In this situation, the choice of the initial density and velocity distribution becomes of paramount importance for constructing a plausible nebula model. The folowing three sections describe the progressive refinement of the initial conditions used to model the solar nebula.

3. FIRST SET OF MODELS

3.1. *Initial Conditions*

In the first set of models, the initial cloud is spherically symmetric, and has power-law density and radial velocity profiles appropriate for gas in free-fall onto a protostellar core (Shu 1977)

$$\rho(r) = \rho_R (R_R/r)^{3/2}, \tag{6}$$

$$v_r(r) = -v_{r1}(R_1/r)^{1/2}, \tag{7}$$

where r is the spherical coordinate radius, R_R is the cloud boundary, and $R_1 = 1$ AU. That is, we are assuming that the central protostar has already formed, and that we can follow just the collapse of the remaining molecular cloud material. In order to form a disk, of course, the cloud must be rotating as well. The initial angular velocity has a profile

$$\Omega(r) = \Omega_R (R_R/r) \tag{8}$$

chosen to resemble that in collapsing clouds (Tscharnuter 1987). Note that the initial angular velocity is not constant on

cylinders, nor need it be, because the initial cloud is not intended to represent an equilibrium configuration.

The initial temperature is defined by a power law profile $T \propto r^{-\alpha}$ chosen so that the cloud is neither heating or cooling initially, i.e., $J = B$. This ensures a stable initial solution for the radiative transfer equation. From the mean intensity equation,

$$f \frac{1}{\kappa\rho} \nabla \cdot \left(\frac{1}{\kappa\rho} \nabla J \right) = J - B \,, \tag{9}$$

so $J = B$ requires that (in spherical symmetry)

$$\frac{d}{dr} \left(\frac{r^2}{\kappa\rho} \frac{dJ}{dr} \right) = 0 \,. \tag{10}$$

With $\rho \propto r^{-3/2}$ and $\kappa \propto T^2$ (Lin & Papaloizou 1980; Pollack, McKay, & Christofferson 1985), this leads to $J \propto r^{-(2\alpha + 5/2)}$. Since $J = B = \sigma T^4/\pi$, we obtain $\alpha = 5/4$, and the desired initial temperature profile is then

$$T(r) = T_1 (R_1/r)^{5/4} \,. \tag{11}$$

3.2. *Results*

Over 50 models were computed starting from these initial conditions. The detailed results for one representative model will be presented here. Model I-e had $\rho_R = 2.7 \times 10^{-14}$ g cm^{-3}, $v_{r1} = 1.0 \times 10^6$ cm s^{-1}, $\Omega_R = 1.2 \times 10^{-9}$ rad s^{-1}, $T_1 = 1500$ K, $\tau_c = 10$, J_R given by equation (4), $f = \frac{1}{3}$, and $R_R = 50$ AU. With these parameters, model I-e had a cloud mass of 0.048 $M_\odot$ and an average specific angular momentum $\langle J/M \rangle = 2.7 \times 10^{20}$ cm^2 s^{-1}, as is appropriate for a minimum mass solar nebula (Safronov & Ruzmaikina 1985). The mass accretion rate onto the central protostar was $\dot{M}_s \sim 6 \times 10^{-4}$ $M_\odot$ yr^{-1}, which is still much too high for low-mass protostars beginning their collapse from a molecular cloud core with a peak density of $\sim 10^{-19}$ g cm^{-3}, for which the free-fall time of $\sim 2 \times 10^5$ yr implies that $\dot{M}_s \sim 5 \times 10^{-6}$ $M_\odot$ yr^{-1}. However, the central temperature was limited in this as well as all the models to being less than or equal to 1700 K, so the disk did not experience as much heating from the central star as would be expected for this high $\dot{M}$.

The results for model I-e after about a year of evolution are shown in Figure 1. A rotationally flattened, optically thick nebula begins to form, extending out to distances of about 3 AU (Fig. 1*a*). The initial temperature profile quickly relaxes to a quasi-steady state determined by the heating and cooling processes in the nebula. Because of the importance of the central luminosity and the chosen initial conditions, the nebula temperature distribution (Fig. 1*b*) remains nearly spherically symmetrical (as in Tscharnuter 1987 and Bodenheimer et al. 1990) as compared to the strong vertical temperature gradients encountered in previous three-dimensional nebula models (Boss 1988, 1989) that did not include these effects. Hence there is no particular concern for these models with regard to resolving the vertical thermal structure of the nebula; a sharp jump in temperature does not yet exist (see § 5.4).

The initial and final midplane temperature profiles for model I-e are displayed in Figures 1*c* and 1*d*, respectively. Relatively high temperatures ($T_m \approx 1500$ K inside 3 AU) are evident, while the midplane temperatures drop below 150 K outside about 5 AU.

The other models in the first set had variations in a large number of parameters: strength of artificial viscosity ($C_Q = 0$ or 1), J boundary condition (see § 2.3), outer radius ($R_R = 25$ or 50 AU) and hence $\langle J/M \rangle = 6.8 \times 10^{19}$ cm^2 s^{-1} or 2.7×10^{20} cm^2 s^{-1}, density ($\rho_R = 1.0 \times 10^{-15}$ g cm^{-3} to 2.7×10^{-14} g cm^{-3}), velocity ($v_{r1} = 1.0 \times 10^6$ cm s^{-1} or 4.2×10^6 cm s^{-1}), Eddington factor ($f = \frac{1}{3}$ or 1), and critical optical depth ($\tau_c = 10$, 5, or 1). Variations in the initial density lead to initial cloud masses (within 25 AU) ranging from ~ 0.0002 to 0.02 $M_\odot$ and to central mass accretion rates from $\dot{M}_s \sim 10^{-5}$ to 6×10^{-4} $M_\odot$ yr^{-1}.

The models with $\dot{M}_s \sim 10^{-5}$ $M_\odot$ yr^{-1} are of the most interest and produced the greatest change in temperatures. Temperature profiles in these models were significantly lower than in model I-e (e.g., $T \approx 850$ K at 1 AU, and ~ 500 K at 2 AU), as might be expected. However, the disk masses in these models were quite low—0.0002 $M_\odot$, and had a maximum (midplane) optical depth of only ~ 5 (vs. ~ 300 for model I-e), so these models cannot be expected to retain compressional heat to the same extent as a more optically thick disk with a mass closer to the minimum mass nebula. Furthermore, because of the low optical depths, the time step restraint (eq. [5]) prevented the models from being calculated even as far in time as model I-e in the sense of producing a rotationally flattened disk. These shortcomings can be traced to the assumption of initially spherically symmetric, infalling clouds—with that assumption, and even with rapid rotation, much of the mass continues to fall onto the central protostar, producing a high $\dot{M}_s$, rather than into the midplane to form the desired disk.

4. SECOND SET OF MODELS

4.1. *Initial Conditions*

The second set seeks to improve on the first set by realizing that most of the late-arriving, high angular momentum gas should not be able to accrete directly onto the protosun. This is especially true if the protosun had an energetic stellar wind (most likely a bipolar flow) that swept out large regions of circumstellar space, e.g., near the rotation axis. Hence the second set started from a nonspherical, disklike cloud already flattened about the midplane, and with the initial flow being toward the midplane.

Cassen & Moosman (1981) derived ballistic trajectories for infalling matter that are appropriate for hypersonic flow onto a point mass. The trajectories are dependent on the angular momentum distribution in the infalling cloud, which is difficult to specify precisely given our poor knowledge of differential rotation in molecular cloud cores. Here we will take a slightly different approach, and approximate the streamlines onto the disk through a simple prescription based on total energy conservation. A parcel of gas infalling from rest at infinity on a ballistic trajectory toward a protostar of mass M_s will have a velocity v given by

$$v^2 = \frac{2GM_s}{r} = v_r^2 + v_\theta^2 + v_\phi^2 \,. \tag{12}$$

We will assume that the angular velocity of the infalling gas is such as to lead to Keplerian rotation at the disk midplane, an assumption that will then minimize any heating due to rotational shear between the infalling gas and the near-Keplerian disk. This assumption is consistent with trying to find a lower bound on nebula temperatures. Choosing the angular velocity to be such that

$$v_\phi = \left(\frac{GM_s}{r} \right)^{1/2} \,, \tag{13}$$

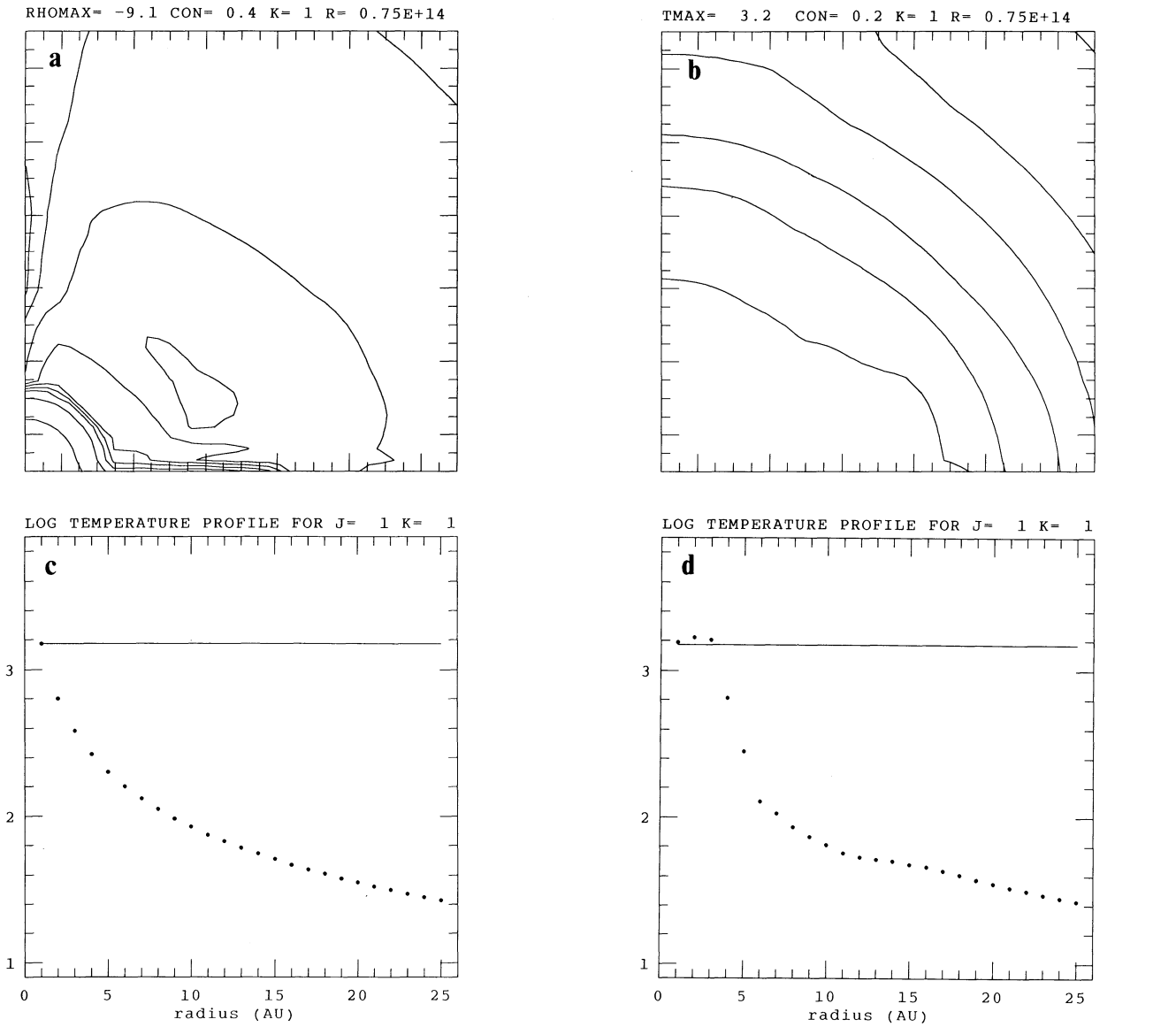

FIG. 1.—Azimuthal plane log density (*a*) and log temperature (*b*) contours for model I-e, and log midplane temperature as a function of radius initially (*c*) and at the same time (*d*) as (*a*) and (*b*). For (*a*) and (*b*), the region shown is 5 AU in radius. The rotation axis falls at the left border, and the midplane at the bottom. Contour intervals correspond to factors of 2.5 change in density and 1.6 in temperature. Logarithms of the maximum values are noted on each plot. The sink cell is evident at the lower left corner of (*a*). A thin disk has built up to a radius of about 3 AU (θ grid points are concentrated toward the midplane). The initial temperature profile (*c*) quickly relaxes to quasi-steady state values (*d*). The horizontal line is 1500 K, which approximates temperatures produced by the thermostatic buffering effect of the dust grain opacity.

conservation of energy is assured if we further choose

$$v_r = -\left(\frac{GM_s}{r}\right)^{1/2} \cos\theta\,, \tag{14}$$

$$v_\theta = \left(\frac{GM_s}{r}\right)^{1/2} \sin\theta\,. \tag{15}$$

With these choices, the translational (v_r, v_θ) velocity field is simply one of vertical infall toward the disk midplane (see Fig. 2*a*), with half of the kinetic energy being in rotational motion and half in translational motion. For a disk with a total radius much larger than the region (10 AU) under consideration in the second set of models, the Cassen & Moosman (1981) ballistic trajectories predict that the innermost streamlines are approximately vertical but with a small deflection toward the central protostar.

The initial density was chosen to yield a disklike configuration with a maximum density at the midplane

$$\rho(r, \theta) = \rho_1(R_1/r)^{3/2}[\theta \sin\theta]^m\,, \tag{16}$$

with $m = 2$ to 10 being varied in order to minimize $\dot{M}_s$. The initial temperature profile was the same as in the first set of models (eq. [11]).

4.2. *Results*

Ten models were computed using initial conditions of this form. It was found that m had to be quite large in order to deplete the gas from the region of the rotational axis enough to

produce a low $\dot{M}_s$. Results from a model with high m are shown here. Model II-e had $m = 10$, $\rho_1 = 1 \times 10^{-10}$ g cm^{-3} (with a minimum density of 10^{-14} g cm^{-3}, where eq. [16] would lead to a lower density), $M_s = 1\ M_\odot$ (which also defines the initial velocity field through eqs. [13]–[15]), J_R is given by equation (4), $C_Q = 0$, $T_1 = 1500$ K, $R_R = 10$ AU, $\tau_c = 10$, and $f = 1$. This model had $\langle J/M \rangle = 1.1 \times 10^{20}$ cm^2 s^{-1}, an initial disk mass of 0.0055 $M_\odot$, and $\dot{M}_s = 2.5 \times 10^{-5}\ M_\odot$ yr^{-1} initially. Partway through the evolution, all available matter was accreted by the protosun, and $\dot{M}_s = 0$ for the rest of the evolution. By contrast, identical models except for having $m = 2$ initially had $\dot{M}_s = 4 \times 10^{-4}\ M_\odot$ yr^{-1}, a value that did not decrease significantly for the duration of the calculation—so the models with low m are not of interest for low-mass star formation.

The results for model II-e are shown in Figures 2 and 3. Figure 2 shows that the initial density configuration undergoes significant flattening toward the midplane even during the relatively short (~0.1 yr) duration of the calculation. Figure 3 shows that the temperature field rapidly adjusts to the asymmetric disk configuration, and produces a mushroom-shaped distribution with highest temperatures in the disk midplane. Quite high midplane temperatures (>2000 K) are produced, and the region with these high temperatures moves continuously outward during the evolution—i.e., it does not appear to reach a quasi-steady state, because the disk continues to compress toward the midplane (note the large vertical velocities within the disk in Fig. 2*c*). The model II-e disk as well as the other models of this type appeared to be convectively stable except for a few isolated locations.

While these models produced quite hot inner disks, the fact that a steady state temperature distribution was not reached and that the disk continued to contract vertically means that these models are still not appropriate for the solar nebula. The

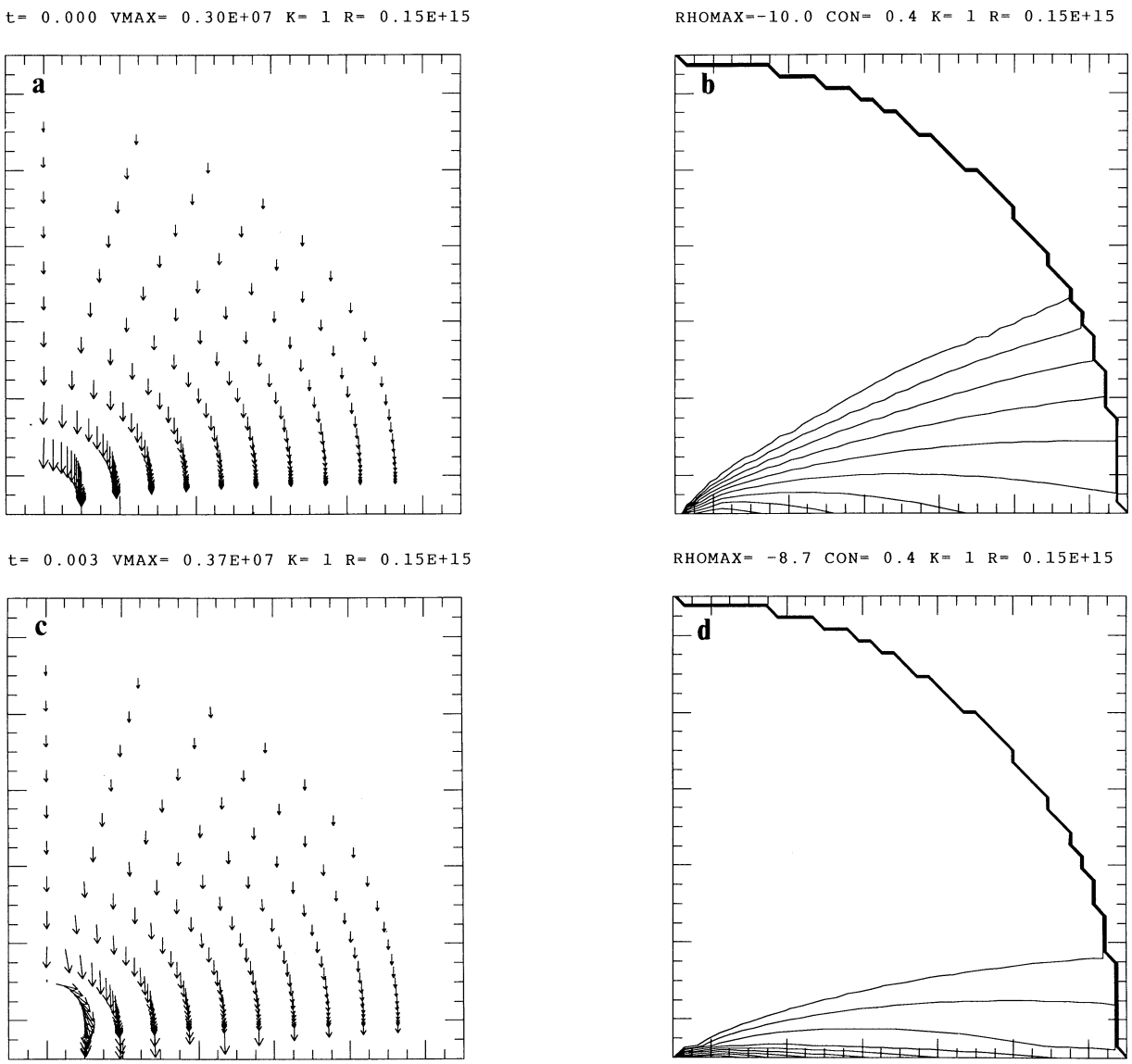

FIG. 2.—Initial velocity field (*a*) and log density contours (*b*) for model II-e and at the end of the calculation [(*c*) and (*d*), respectively]. Velocities are plotted at every fifth grid point in radius. Region shown is 10 AU in radius. Density contour levels correspond to factors of 2.5 change; maximum velocities in cm s^{-1} are noted at the top. Considerable vertical contraction of the initial disk is evident.

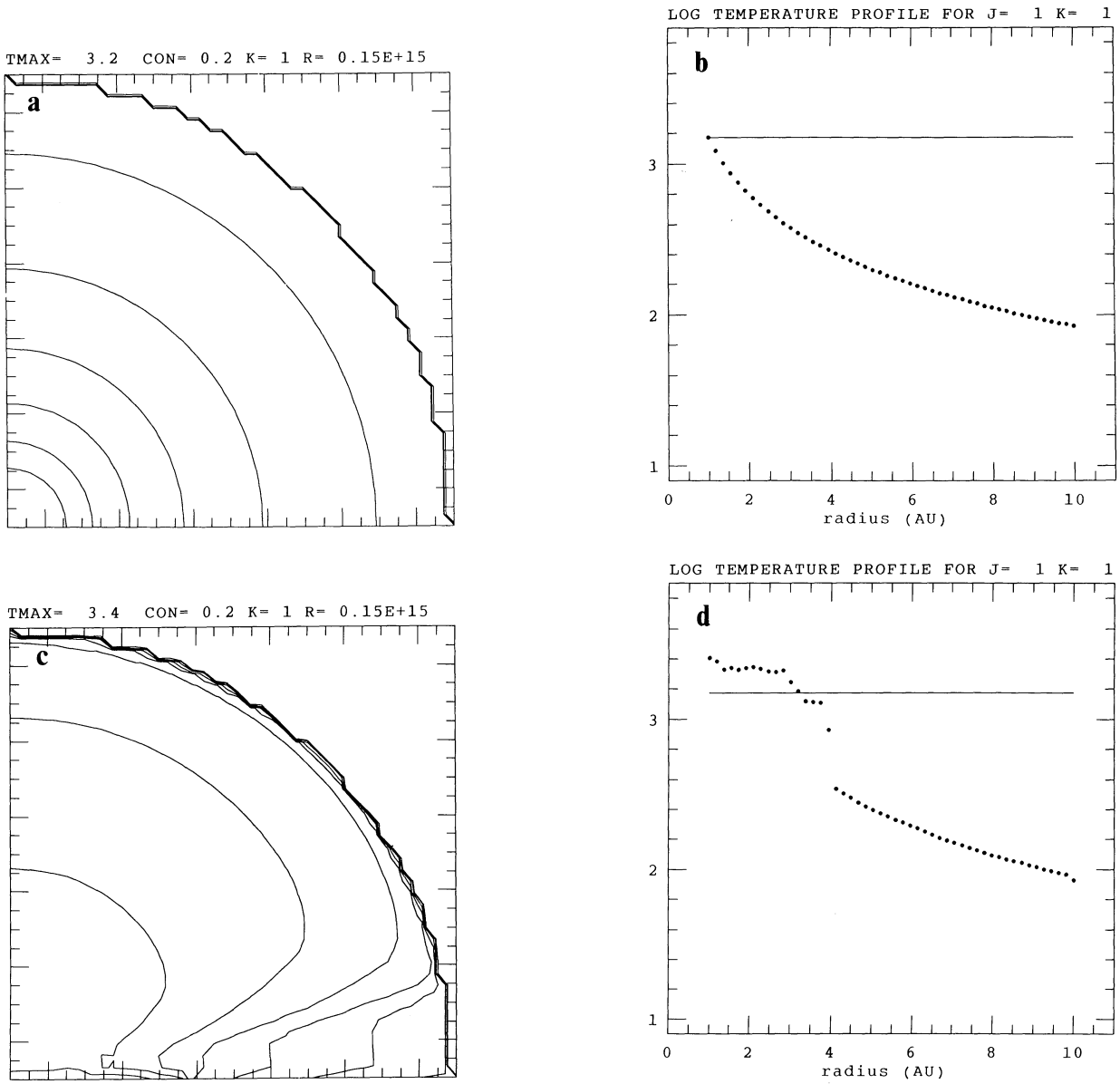

FIG. 3.—Initial log temperature contours (*a*) and log midplane temperature (*b*) for model II-e and at the end of the calculation [(*c*) and (*d*), respectively]. Region shown is 10 AU in radius. Temperature contour levels correspond to factors of 1.6 change. Horizontal line in (*b*) and (*d*) is $T = 1500$ K. The initial spherically symmetric temperature profile quickly produces a distribution (*c*) composed of a thin disk component centered on the midplane (bottom border) and a mushroom cap of radiatively heated gas above the disk. Relatively high midplane temperatures (*d*) are produced out to 4 AU because of the rapid vertical compression of the disk.

problem is simply that because of the ad hoc choice of the initial density, designed primarily to minimize $\dot{M}_s$, the resulting disks undergo a very rapid contraction and hence vigorous compressional heating. In effect, the disks are being formed too rapidly in these models, based on our understanding of low-mass star formation. This can be quantified by calculating the mass flux into a control volume drawn around the disk and so defining the disk mass accretion rate

$$\dot{M}_d \approx 2 \times 10^{-2}\ M_\odot\ \mathrm{yr}^{-1} \left(\frac{v_z}{10\ \mathrm{km\ s}^{-1}}\right)\left(\frac{R_R}{10\ \mathrm{AU}}\right)^2 \times \left(\frac{\rho_h}{10^{-11}\ \mathrm{g\ cm}^{-3}}\right), \quad (17)$$

where v_z is the vertical infall velocity just above the disk surface and ρ_h is the "halo" density of the matter infalling onto the disk. For the nominal values in equation (17), $\dot{M}_d \sim 10^{-2}\ M_\odot$ yr^{-1}, a rate that is still too high for low-mass star formation, because we expect that for a steady state accretion process where molecular cloud infall is feeding the disk and the disk is accreting onto the protostar, $\dot{M}_s \sim \dot{M}_d \sim 10^{-6}$–$10^{-5}\ M_\odot$ yr^{-1}. This deficiency is remedied in the third and final set of models.

5. THIRD SET OF MODELS

5.1. *Initial Conditions*

In order to avoid having the disk form too rapidly, the third set of models starts from an approximate equilibrium state for

an adiabatic, self-gravitating, "fat" (nonthin) disk in near-Keplerian rotation about a protosun. The Appendix derives the following approximate vertical density distribution for such a configuration

$$\rho(R, Z)^{\gamma-1} = \rho_0(R)^{\gamma-1} - \left(\frac{\gamma-1}{\gamma}\right)\left\{\left[\frac{2\pi G\sigma(R)}{K}\right]Z + \frac{GM_s}{K}\left[\frac{1}{R} - \frac{1}{(R^2+Z^2)^{1/2}}\right]\right\}, \quad (18)$$

where R and Z are cylindrical coordinates, $\rho_0(R)$ is the midplane density, and $\sigma(R)$ is the disk surface (mass) density. The adiabatic pressure is defined by $p = K\rho^\gamma$, where K is the adiabatic constant and γ is the adiabatic exponent. Note that the adiabatic pressure relation is used solely to define the initial disk model; the actual calculation still solves the radiative transfer equation.

The Appendix points out that a natural choice for the radial density dependence results from the condition that the contribution of the gas pressure to non-Keplerian rotation be small everywhere in the disk. For a power-law midplane density, $\rho_0(R) \propto R^{-a}$, the Appendix shows that this choice leads to $a = 1/(\gamma - 1)$. For temperatures of 100 K or less, para hydrogen is expected to dominate, so that the rotational levels of molecular hydrogen do not contribute to the internal energy (e.g., Boss 1984), and as a result the effective value of γ is 5/3 rather than the value of 7/5 normally expected for a diatomic molecule. The choice $\gamma = 5/3$ leads to $a = 3/2$, and so the midplane density is defined by

$$\rho_0(R) = \rho_{01}\left(\frac{R_1}{R}\right)^{3/2}, \quad (19)$$

where $\rho_{01} = 4.0 \times 10^{-10}$ g cm^{-3}. For a disk whose vertical height increases linearly with radius, as is approximately true for equation (18), the surface density of the disk then varies as

$$\sigma(R) = \sigma_1\left(\frac{R_1}{R}\right)^{1/2}, \quad (20)$$

where $\sigma_1 = 2.0 \times 10^3$ g cm^{-2} is determined by numerically integrating equation (19). The adiabatic constant was given the value $K = 1.7 \times 10^{17}$ (cgs units), based on $\gamma = 5/3$ and the fact that protostellar gas first begins heating above the cold molecular cloud value of 10 K for densities greater than about 10^{-13} g cm^{-3}. With these choices, the disk surface lies at an angle of $\approx 13°$ above the midplane.

In addition to the disk density structure defined by equation (19), a low-density halo is introduced into the region above the disk surface, in order to simulate the remaining infalling molecular cloud material, of the form

$$\rho_h = \rho_{h1}\left(\frac{R_1}{r}\right)^{3/2}, \quad (21)$$

where $\rho_{h1} = 1.0 \times 10^{-14}$ g cm^{-3}.

The outer radius for these models was 10 AU, leading to a disk mass of 0.020 $M_\odot$. For comparison, the minimum mass nebula (Weidenschilling 1977) has about 0.005 to 0.035 $M_\odot$ contained within 10 AU, about $\frac{1}{2}$ the total nebula mass. The initial conditions result in $\dot{M}_s \rightarrow 0$ rather early in the calculations, and using equation (17) with an effective $\rho_h \sim 10^{-15}$ g cm^{-3}, these models have $\dot{M}_d \sim 10^{-6}$ to 10^{-5} $M_\odot$ yr^{-1}, as desired.

The initial velocity field is specified as in the second set of models by equations (13) through (15), with $M_s = 1$ $M_\odot$. The initial velocity field vanishes inside the disk, as before. The average specific angular momentum of the disk was $\langle J/M \rangle = 1.0 \times 10^{20}$ cm^2 s^{-1}. The models also had $\tau_c = 10$, $C_Q = 1$ (except for III-l), J_R determined by equation (4), and $f = 1$.

The initial temperature profile was taken to be spherically symmetrical with a power-law dependence

$$T(r) = T_1(R_1/r)^\alpha, \quad T(r) \leq T_U, \quad (22)$$

where the exponent α, normalizing factor T_1, and temperature upper limit T_U were varied from model to model. The temperature upper limit was used in order to produce initial profiles resembling those resulting from the thermostatic effect of the dust grain opacities (Morfill 1988; Boss 1990).

As discussed in § 2.4, limitations on the time step mean that these models are primarily intended to search for a steady state thermal distribution. That is, a variety of initial temperature distributions are investigated, and the calculation is then evolved far enough that a quasi-steady state thermal distribution is reached. If this distribution is hotter than the initial guess, then the initial guess is assumed to be too low. In order to map out the possible temperature profiles in the inner nebula, 13 models of the third type were calculated—the variations explored are listed in Table 1. Another nine models were calculated to determine the sensitivity of the results to changes in other parameters.

5.2. *Results*

Figure 4 shows the results for a model (III-t) that has an initial temperature profile that is close to that derived from the whole set of models for the steady state midplane distribution. The low-density halo begins to accrete onto the disk, with the low angular momentum gas along the rotational axis being accreted first. The disk itself contracts slightly during the evolution. The temperature field rapidly readjusts to a quasi-equilibrium value; by the end of the calculation ($\sim\frac{1}{3}$ yr), the temperature has essentially stopped evolving. (The final temperature contour plots in Figs. 4 and 6 were smoothed near the rotational axis to remove numerical artifacts associated with the symmetry axis.) The lowest temperatures are obtained along the rotational axis ($\tau \sim 10^{-2}$), with the highest temperatures occurring inside the disk ($\tau \sim 10^4$). The midplane

TABLE 1

INITIAL CONDITIONS FOR THE THIRD SET OF NEBULA MODELS

Model	α	T_1 (K)	T_U (K)
III-j	5/4	5000	1500
III-k	5/4	3000	1500
III-m.....	5/4	2000	1500
III-i	5/4	1500	1500
III-h	5/4	1000	1500
III-r	5/4	5000	1400
III-s	5/4	4000	1400
III-t	5/4	3000	1400
III-u	5/4	2000	1400
III-n	7/4	5000	1500
III-o	7/4	4000	1500
III-p.....	7/4	3000	1500
III-q.....	7/4	2000	1500

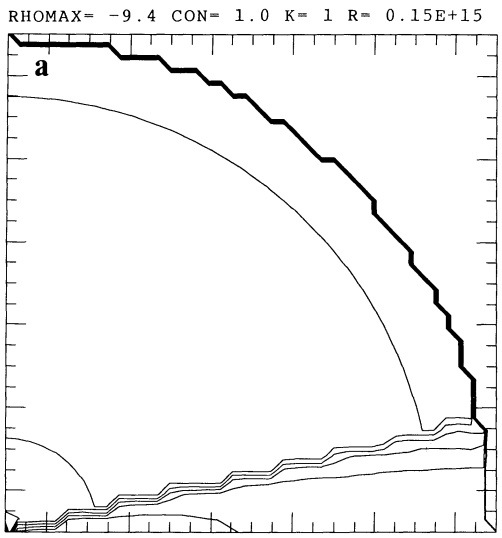

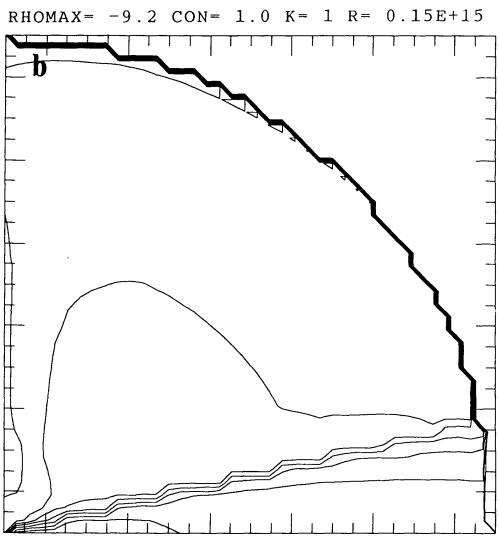

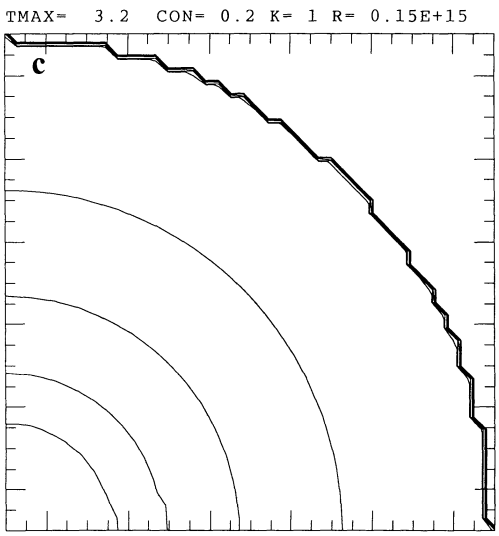

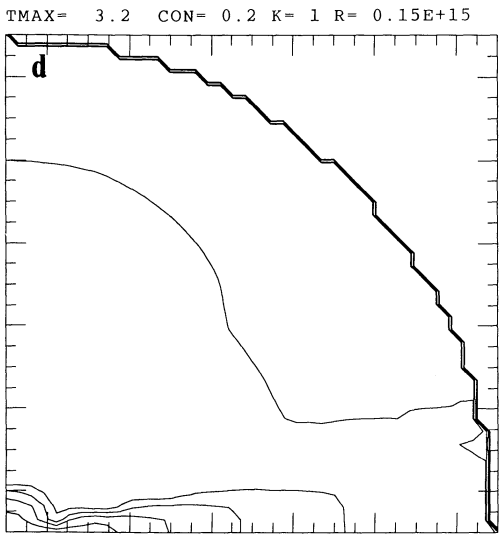

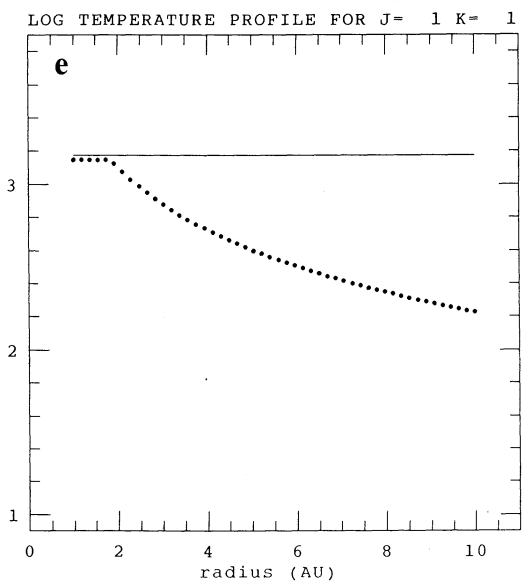

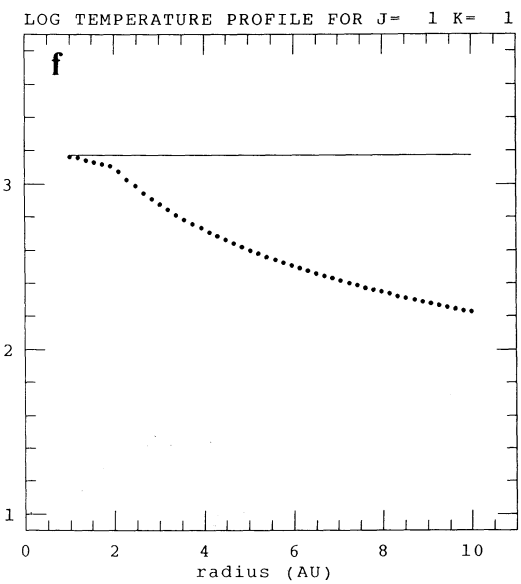

temperature changes only slightly, rising above 1400 K around 1 AU and dropping below 1400 K around 2 AU.

The final model for III-t is convectively stable except at a few isolated grid points. While nebula models are generally expected to be convectively unstable in the vertical direction (Lin & Papaloizou 1980), the apparent stability of these models may be partially due to the initial temperature profile being approximately isothermal in the vertical direction, and to the final models not necessarily being completely relaxed to the true equilibrium distribution. A vertically isothermal nebula has a temperature gradient (zero) less than the adiabatic value and so is convectively stable.

The sources of compressional heating for these models are (i) infall of the halo onto the disk, (ii) vertical contraction of the disk, (iii) accretion onto the protosun that leads to the inner boundary temperature of 1700 K, and (iv) heating due to artificial viscosity. Thermal energy is lost primarily through (v) radiation from the disk (a small component goes into internal energy of the gas). It is important to understand the role played by each of these five factors, in order to assess the physical reality of the results. Nine models were calculated with variations intended to test each of these factors.

(i).—Models III-ad and III-ae had ρ_h increased or decreased by a factor of 3, respectively. Both final models had midplane temperatures that were nearly identical to model III-t, but at 2 AU III-ad had a temperature of 256 K just above the disk surface, versus 218 K for III-ae and 226 K for III-t, as expected. Thus the interior disk temperatures are not strongly dependent on the precise choice of the halo density. This is presumably due to the fact that much of the accretional energy produced at the disk surface by halo infall is immediately lost through radiation [see also (v) below]. The main thermal effect of the mass added by the halo may be through its addition to the mass inside the disk and the consequent vertical contraction within the disk, where the compressional energy produced can be more readily retained than at the disk surface.

(ii).—Models III-w, III-x, III-aa, and III-ac had translational velocities within the disk arbitrarily decreased (without resulting in disk heating) by factors of 0.99, 0.999, 0.9999, and 0.99999 each time step, respectively. The intent was to slow down the rate at which the disk contracts without contributing to disk heating. The disk contracts (primarily in the vertical direction) because of mass added to the top surface by accretion from the halo, and because the initial temperature profile defined by equation (22) differs in general from that implicitly used to generate the density distribution through equations (18) and (19), i.e., the initial disk is not quite in equilibrium for an arbitrary temperature profile, and may expand or contract. At 2 AU, the average vertical contraction velocities in the final disks were: 760 cm s^{-1} for model III-t, 78 cm s^{-1} for model III-ac, 4.5 cm s^{-1} for model III-aa, 1.0 cm s^{-1} for model III-x, and 0.22 cm s^{-1} for model III-w. Models III-w and III-x cooled from 1400 to 1390 K and 1398 K at 1 AU, respectively, while models III-aa, III-ac, and III-t heated from 1400 K to 1407, 1447, and 1454 K at 1 AU, respectively, indicating that disk contraction is an important heating effect. For a disk gaining mass at a rate of $10^{-5}\ M_\odot\ yr^{-1}$, an equation similar to equation (17) shows that vertical contraction of the disk caused by the added mass should lead to $v_Z \sim 150$ cm s^{-1}, a value intermediate between the average values for models III-t and III-ac. Considering the small difference in final temperature between these two models, it would appear that the heating due to disk contraction in the standard models is approximately correct.

(iii).—Model III-y had an inner temperature of 1500 K instead of the standard choice of 1700 K. The final midplane temperature for III-y was nearly identical to that of III-t, indicating that small changes in the central temperature do not greatly affect the disk temperature.

(iv).—Model III-l had $C_Q = 0$ but was otherwise the same as model III-m, and produced midplane temperatures only slightly smaller (e.g., 795 K vs. 799 K at 2 AU) than model III-m. Evidently heating due to artificial viscosity also has only a small effect.

(v).—Model III-v had the radiative fluxes throughout the grid multiplied by an arbitrary factor of 3, in order to assess the importance of the accuracy of the radiative fluxes (see also § 5.4). The luminosity of model III-v was about 1.2 times higher than in III-t, and the midplane temperatures were again slightly lower (e.g., 1181 K vs. 1186 K at 2 AU) than in III-t. Just below the disk surface, somewhat larger differences were found: 804 K in III-v versus 830 K in III-t at 2 AU. This model implies that the midplane temperatures are not strongly dependent on the radiative fluxes, because the radiative losses occur largely at the nebula surface, and not at the optically thick midplane [see (i) above] where the radiative flux is small.

5.3. *Composite Model*

In order to avoid any problems associated with the final temperature distributions not being exact equilibrium solutions, the standard models in Table 1 were used to determine a "composite" midplane temperature. The assumption is that if the final midplane temperature for the model was greater than the initial temperature at a certain radius, then the initial guess was probably too low. Figure 5*a* shows the results for all 13 models in Table 1. There is a clear demarcation inside 5 AU between initial profiles that appeared to be too low and those that were too high, and this demarcation defines the composite profile shown in Figure 5*b*. Note that temperatures barely changed in the midplane outside 5 AU, so the midplane temperature profile is not well-constrained in this region and has been arbitrarily chosen to approach 100 K at 10 AU. The structure in the composite profile is apparently caused by thermostatic behavior associated with the evaporation of three dominant contributors to the opacity (Pollack et al. 1985): (i) high-temperature silicates and Fe around 1300 K; (ii) low-temperature Fe-bearing silicates around 350 K; and (iii) water ice around 150 K.

A final model (III-ab) was evolved starting with a spherically symmetric version of the temperature profile given by Figure 5*b*, in order to produce a composite nebula model, i.e., the "best guess" of all the models presented here. Figure 6 displays the final configuration for this model. The fact that the temperature contours still show evidence of heating at the disk

FIG. 4.—Initial log density contours (*a*), log temperature contours (*c*), and log midplane temperature (*e*) for model III-t and at the end of the calculation [(*b*), (*d*), and (*f*), respectively]. Region shown is 10 AU in radius. Density contour levels correspond to factors of 10 change, and temperature contours to factors of 1.6 change. Jagged contours are artifacts of the plot routine. Horizontal line in (*e*) and (*f*) is $T = 1500$ K. The density distribution of the quasi-equilibrium disk does not change greatly, but the temperature distribution rapidly relaxes to a quasi-steady state with the highest temperatures within the disk. The midplane temperature changes only slightly in the inner regions.

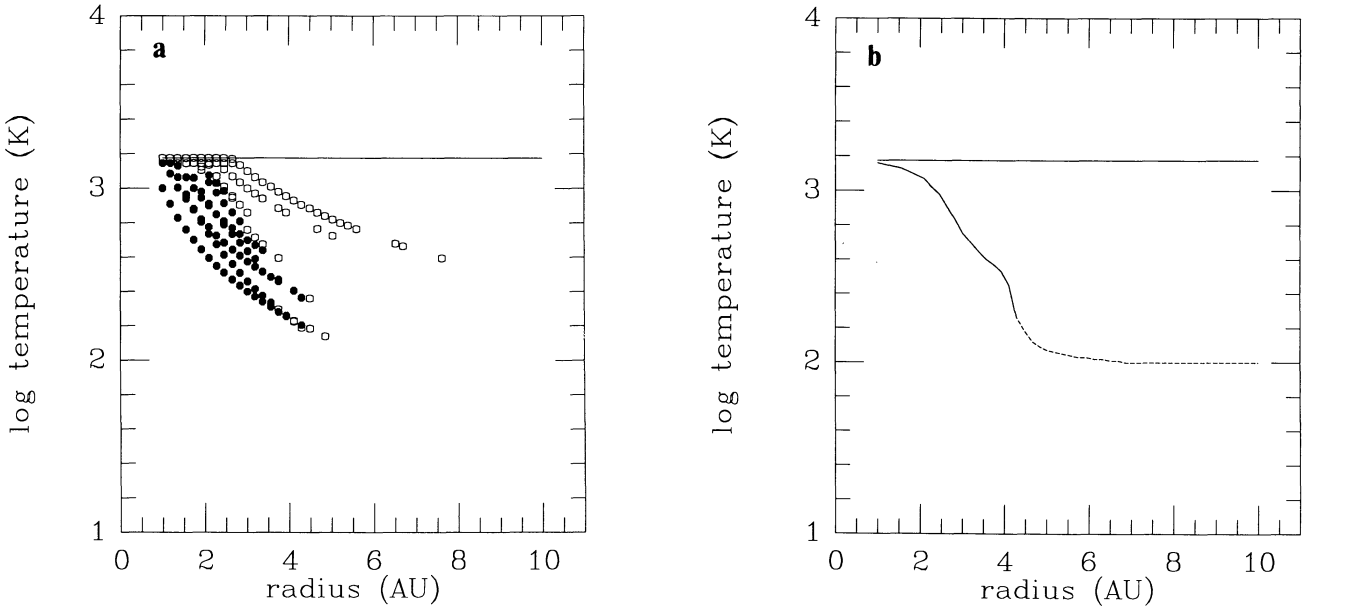

FIG. 5.—Determination of the composite temperature profile from the results of the models in Table 1. For each grid point for each model, a solid circle is plotted in (*a*) if the final temperature increased over the initial temperature, and an open circle if it decreased. No symbol is plotted if the increase in temperature was by less than a factor of 1.001 or the decrease was by less than a factor of 0.999. The intersection between the solid and open symbols defined the composite temperature, shown for clarity in (*b*), including an arbitrary extrapolation to 100 K in the outer nebula.

surface beyond about 6 AU to values above those at the midplane (Fig. 6*b*) indicates that $T \sim 160$ K might be a better value for this portion of the nebula than $T \sim 100$ K.

Figure 7 shows the midplane density and surface density profiles for model III-ab. The models are stable to axisymmetric gravitational perturbations, because according to the Toomre (1964) Q stability criterion, gravitational instability ($Q < 1$) occurs only when $\sigma > \sigma_Q$, where σ_Q is defined by

$$\sigma_Q = 0.936 \frac{c_s \Omega}{\pi G}, \tag{23}$$

where c_s is the sound speed. Figure 7*b* shows that the nebula surface densities are at least an order of magnitude too low for gravitational instability, consistent with the low nebula mass of 0.02 $M_\odot$ and the relatively high nebula temperatures. The surface densities are consistent however with the densities thought to be necessary for Earth formation (Goldreich & Ward 1973) and the rapid formation of Jupiter (Lissauer 1987).

Figure 8 shows the dependence of the pressure on the temperature in model III-ab, a relationship of interest for determining the phase stability of various meteoritical components. It can be seen that the pressure-temperature relation for the composite disk model is intermediate between the adiabatic relation used to define the initial models (with $\gamma = 5/3$) and a typical viscous accretion disk profile (Wood & Morfill 1988). Gas pressures in the inner nebula are on the order of 10^{-6}–10^{-5} atm.

As in the other models, the nebula gas in model III-ab is very nearly in Keplerian rotation. The degree of deviation from Keplerian rotation can be quantified by

$$\delta\Omega = \left| \frac{\Omega_g - \Omega_K}{\Omega_K} \right|, \tag{24}$$

where Ω_g is the angular velocity of the gas and Ω_K is the Keplerian value. For model III-ab, values of $\delta\Omega$ range from $\sim 10^{-3}$ to $\sim 10^{-2}$. These values are quite similar to those previously inferred for solar nebula models (Adachi, Hayashi, & Nakazawa 1976).

5.4. *Radiative Transfer Accuracy*

Stemwedel et al. (1990) have shown the possible importance of an accurate energy budget for determining the dynamical outcome of cloud collapse, i.e., whether rings or disks result. They then worry that in numerical models of collapse, where postshock cooling regions generally cannot be resolved and where the collapsed configuration may span only a few grid cells, shock radiation losses may be underestimated and errors may occur in the properties of the collapsed configurations. The present numerical models were constructed with grids strongly compressed in the θ direction, which should remove the latter concern—e.g., the solar nebula models in this section have fairly well-resolved vertical density structures, containing ~ 14 grid cells from the midplane to the nebula surface. However, even the present models do not resolve the thin postshock cooling (thermal) layer ($\sim 10^{10}$ cm thick, Cassen & Moosman 1981). Here we consider the question of accuracy in the radiative transfer solutions for the present models as well as for previous models of the solar nebula.

All viscous accretion disk models to date employ simple relations based on radiative transfer in optically thick regions to link temperatures at the midplane (T_m) and surface (T_s) of the disk. Pringle (1981) used $T_m^4 = \tau_m T_s^4/4$, where τ_m is the optical depth to the midplane. Cabot et al. (1987) used $T_m^4 = (\frac{1}{2} + 3\tau_m/4)T_s^4$, Morfill (1988) used $T_m^4 = (1 + 3\tau_m/4)T_s^4$, while Ruden & Lin (1986) and Ruden & Pollack (1991) used $T_m^4 = 3\tau_m T_s^4/4$ for optically thick regions, and $T_m^4 = 3\tau_{\rm crit}^2 T_s^4/(4\tau_m)$ for optically thin regions ($\tau_m < \tau_{\rm crit}$), with $\tau_{\rm crit} = 1.78$ for Ruden & Pollack (1991). For large optical depths ($\tau_m \to \infty$), nearly all of these $T(\tau)$ relations yield $T_m^4 \to 3\tau_m T_s^4/4$. Evidently these relations are all based on the equation

$$T^4 = \tfrac{3}{4} T_s^4 (\tau + \tau_0), \tag{25}$$

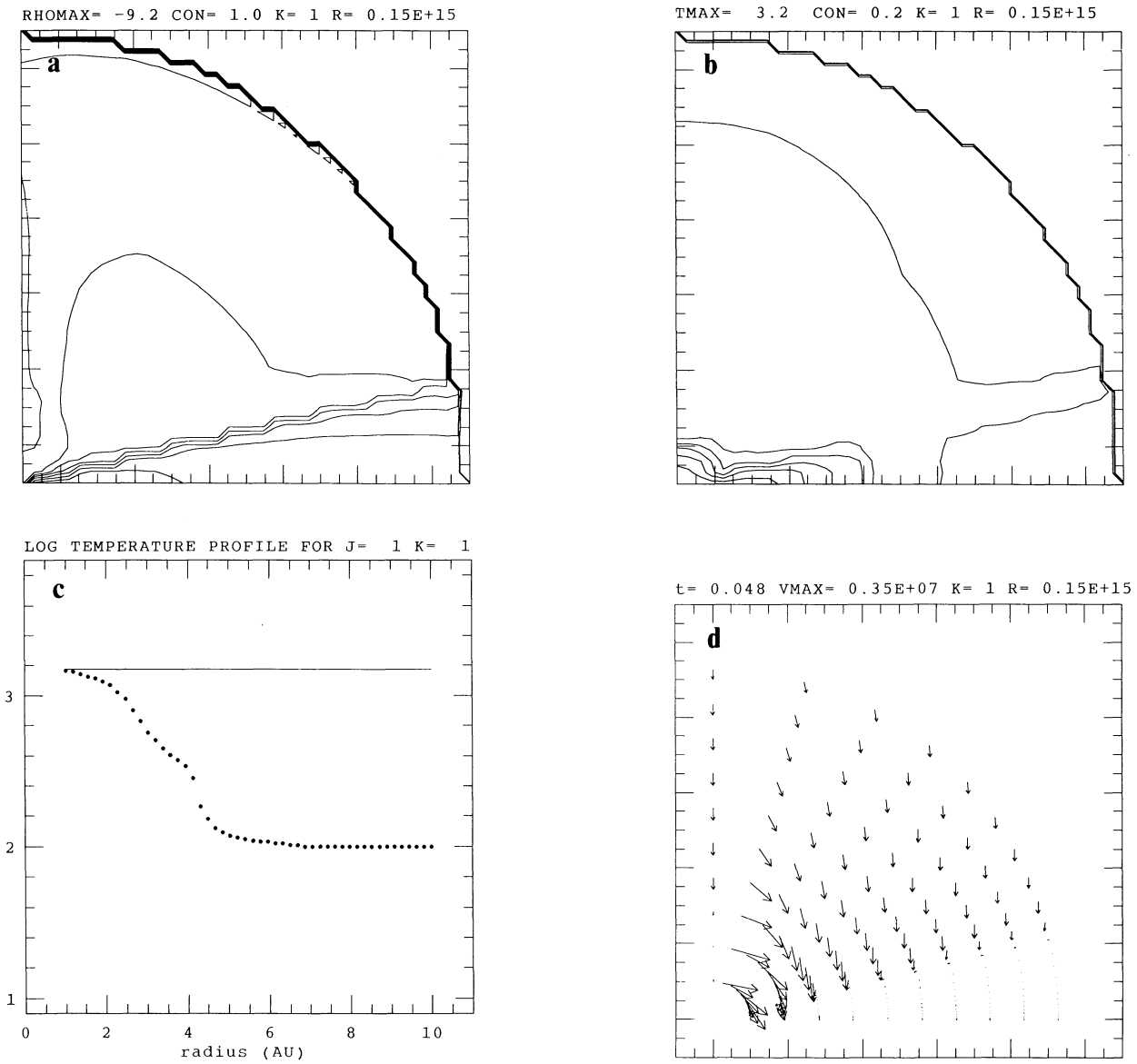

FIG. 6.—Final log density contours (*a*), log temperature contours (*b*), log midplane temperature (*c*), and velocity vectors (*d*) for the composite temperature model III-ab. Region shown is 10 AU in radius. Density contour levels correspond to factors of 10 change, and temperature contours to factors of 1.6 change. Jagged contours are artifacts of the plot routine. Velocity vectors are plotted at every fifth radial grid point. Horizontal line in (*c*) is $T = 1500$ K.

where τ_0 is a constant $\sim\frac{2}{3}$ (e.g., Münch 1960; Shu 1991, p. 32). This relation is derived for steady state, plane-parallel atmospheres with gray opacities and in radiative and local thermodynamic equilibrium. With these assumptions, the temperature-optical depth relation can be specified independently of the atmospheric structure (Shu 1991), but this is not generally the case. Depending on the precise value chosen for τ_0, boundary temperatures derived from this relation can vary by factors of ~ 1.04 (fluxes by factors of ~ 1.2) compared to the exact solution (Shu 1991). The variations in the $T(\tau)$ relation used in the viscous accretion disk models can lead to radiative fluxes ($\propto T_m^4$) that vary by factors of, e.g., 1.5 between the Morfill (1988) and Cabot et al. (1987) relations at $\tau = \frac{2}{3}$ for the same T_s.

Considering that equation (25) was derived for radiative equilibrium, whereas viscous accretion disk models generally invoke the presence of convection to generate turbulence and hence appreciable viscosity, the use of equation (25) is not strictly correct for a turbulent nebula where the vertical structure is affected by convective energy transport (e.g., Schwarzschild 1965). In such a situation the adiabatic temperature gradient generally is more appropriate. The amount of error introduced by this inconsistency has not been quantified as yet. The present nebula models are largely convectively stable, so the use of radiative equilibrium equations (i.e., the Eddington approximation) is justified a posteriori.

The mass and momentum equations of the Rankine-Hugoniot shock jump conditions are automatically satisfied at any shock front in a numerical code that solves the hydrodynamical equations in conservation law form. However, because

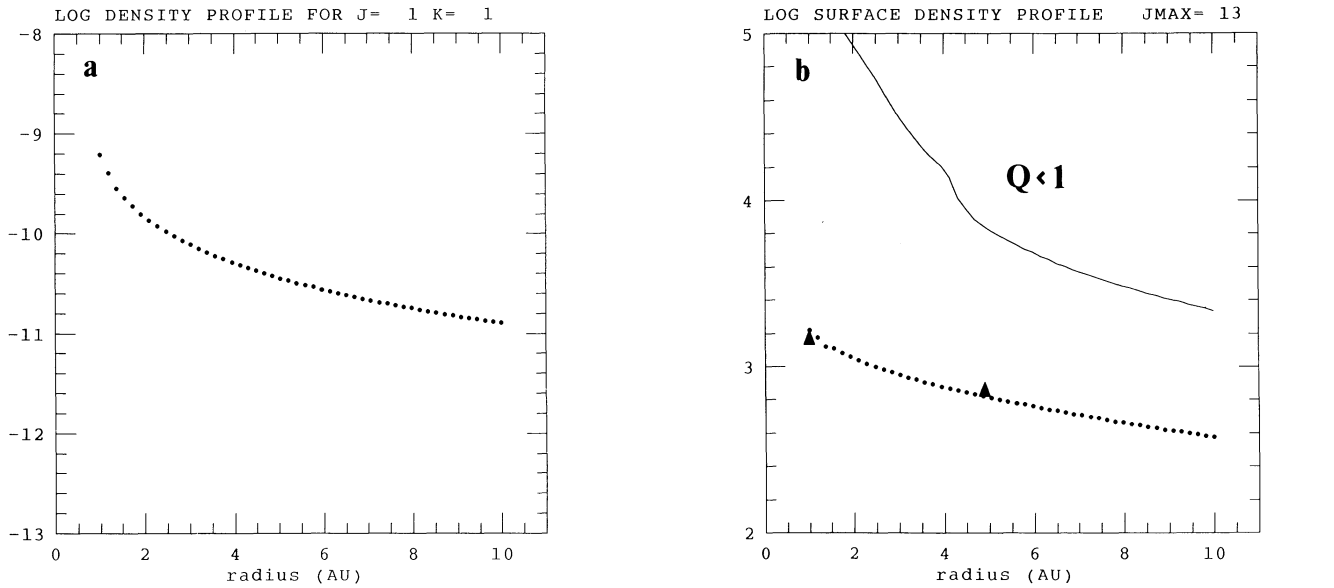

FIG. 7.—Midplane density (*a*) and surface density (*b*) profiles for model III-ab. Solid circles represent model values at each radial grid point. In (*b*), the solid line is the Toomre (1964) Q axisymmetric stability criterion, calculated for the midplane temperature profile of model III-ab. The model values fall well below the Q curve, implying stability ($Q > 1$). Solid triangles in (*b*) represent surface densities assumed for Earth formation by Goldreich & Ward (1973) and for Jupiter by Lissauer (1987).

there is no such conservation equation for the total energy, errors in the energy budget may occur in hydrodynamical calculations.

Shu (1991) points out that erroneous radiative fluxes may arise if shock fronts are numerically spread out over more than a fraction of a photon mean free path. For the present models, the IR photon mean free path $\lambda = 1/\kappa\rho \approx 10^{13}$ cm at the disk surface, whereas the vertical grid spacing is $\sim 10^{12}$ cm there, suggesting that the radiative fluxes from the present models are adequately resolved. The radiative fluxes are dependent on the mean intensity J, and J varies smoothly throughout the disk, dropping to much lower values at the disk surface (similar to the temperature contours).

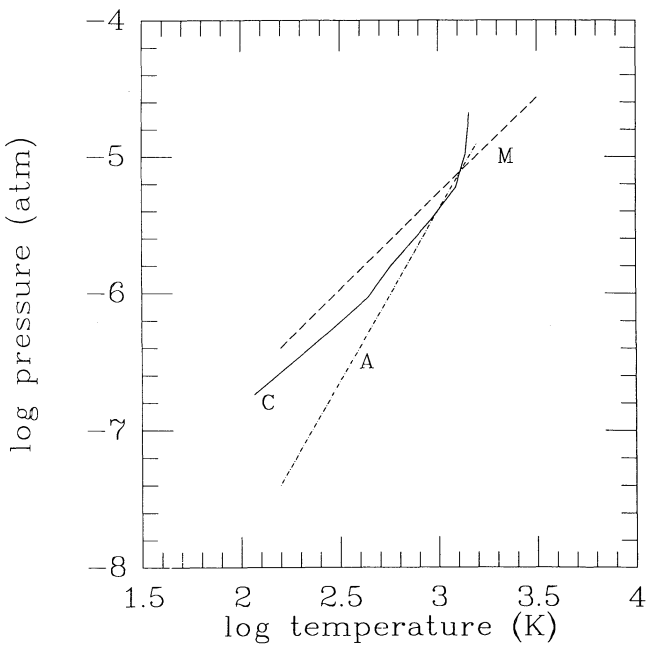

FIG. 8.—Dependence of gas pressure on temperature for the midplane of the composite disk model (C), for the adiabatic relation ($\gamma = 5/3$) used to generate the initial models (A), and for a generic viscous accretion disk model (M) from Wood & Morfill (1988).

Stahler, Shu, & Taam (1980a) describe the detailed thermal structure expected for a protostellar accretion shock, and show that optically thin preshock regions produce shocks that radiate with an effective temperature $T_{\rm eff} \approx 1.07 T_3$, where T_3 is the postshock gas temperature. Given that a multidimensional numerical code may not have enough vertical spatial resolution to be able to distinguish between $T_{\rm eff}$ and T_3 at the disk surface, errors in the surface radiative fluxes could be as high as factors of $1.07^4 = 1.3$. Section 5.2 showed that the midplane temperatures in the present models are fairly insensitive to changes in the global radiative flux by a factor of 1.3. The energy generated at the disk surface is largely lost anyway, and more important for midplane temperatures is the energy produced within the disk by disk contraction fueled by the addition of mass from the infalling halo.

In this context it is interesting to note that the effective temperatures (where $\tau = \frac{2}{3}$) for model III-ab viewed along the rotational axis are about 200 to 350 K, at 4 to 1 AU, respectively (Boss & Yorke 1993). The effective temperatures inferred for a large sample of circumstellar disks at distances of 1 AU from their central young stellar objects range from about 100 to 400 K (Beckwith et al. 1990). The spectral appearance of the composite model III-ab is considered by Boss & Yorke (1993).

6. CONCLUSIONS

The sequence of three sets of solar nebula models shows that increasingly realistic models of the formation phase of a protoplanetary disk orbiting a solar-mass protostar can be constructed and used to determine the thermal structure and other properties of the disk. The third and most realistic set of models shows that a minimum mass ($\sim 0.02\ M_\odot$ within 10 AU) protoplanetary disk undergoing mass accretion at a rate of

$\sim 10^{-6}$–10^{-5} $M_\odot$ yr^{-1} will have midplane temperatures greater than ~ 1000 K inside 2.5 AU and over 1400 K at 1 AU, while falling to ~ 100 K outside 5 AU. While completely independently derived, the calculated model temperatures seem to agree well with interpretations of cosmochemical evidence in favor of moderately high maximum temperatures (~ 1300 K) in the inner solar nebula (Larimer & Wasson 1988; Palme & Boynton 1992), as well as with the lower temperatures (~ 100 K) required at 5 AU and beyond in order for the icy component of the nebula to be able to participate in planetesimal accumulation at an early phase of nebula evolution (Stevenson & Lunine 1988; Wetherill 1990). Because of the strong dependence of the temperatures in the outer nebula on the boundary conditions, the models do not make a firm prediction of temperatures at 10 AU and beyond and so cannot yet be compared to the cometary evidence (Mumma et al. 1992).

The particular density profile chosen for the third set of models leads to a surface density ($\sigma \propto r^{-1/2}$) which is compatible with the high nebula surface densities needed at 5 AU and beyond in order for Lissauer's (1987) runaway accretion scenario to occur. In this scenario, giant planet formation occurs through the rapid ($\sim 10^6$ yr) formation of ice-rock cores that subsequently accrete gaseous envelopes. How the nebula could have reached this surface density profile has not been studied here and remains as an important question for the future; Ruden & Pollack (1991) show how a convectively driven accretion disk may even lead to *rising* profiles ($\sigma \propto r^{1/2}$).

The primary source of heating in these models is compressional energy derived from the collapse of the residual molecular cloud core onto the protoplanetary disk, leading to contraction of the disk itself, and, through the inner boundary condition on the temperature, mass accretion onto the protostar. To the extent that other sources of heating may exist (e.g., viscous or ohmic dissipation, or rotational shear), the temperatures obtained should thus be lower bounds. Energy transport associated with convection is not a significant contributor to these models because of their general convective stability. Thermal energy is lost primarily through radiative losses to the cool surroundings of the nebula. Once mass accretion onto the nebula is terminated, the nebula will cool significantly below the calculated values. It is not yet known to what extent solids derived from the mass-accreting nebula phase and those from the following (cooler) phases contribute to the formation of planetesimals and asteroids.

The composite midplane temperature profile (Fig. 5*b*) is similar to that derived by Cassen (1992) using observations of young stellar objects, except that model III-ab is somewhat cooler throughout (e.g., in the Cassen 1992 model, $T = 100$ K falls well outside 10 AU). A separate paper (Boss & Yorke 1993) demonstrates that model III-ab, when combined with a disk model similar to that used by Adams, Emerson, & Fuller (1990), yields a remarkably good fit for the entire spectrum of T Tauri N and its protoplanetary disk.

I thank Pat Cassen, Herbert Palme, John Wasson, and George Wetherill for stimulating discussions about nebula properties. The referee provided valuable comments on the meteoritical evidence. The calculations were performed on the HP/Apollo DN-10040 workstation of the Carnegie Institution of Washington. This research was partially supported by National Aeronautics and Space Administration grant NAGW-1410.

APPENDIX

We desire an analytical expression for the vertical hydrostatic equilibrium of an adiabatic ($p = K\rho^\gamma$), self-gravitating disk with arbitrary thickness, in near-Keplerian orbit about a central point mass (M_s). An exact expression for such a configuration does not exist, but in this Appendix we use a combination of two analytical expressions for similar configurations in order to approximate the desired structure. We then suggest a particular choice for the radial variation of the disk.

A1. KEPLERIAN DISK

Here we find the vertical equilibrium structure for an arbitrary thickness, adiabatic, non–self-gravitating disk in Keplerian rotation about a central point mass. The radial structure is assumed to be locally constant, because with the assumption of pure Keplerian rotation there can be no radial pressure gradient at the midplane. The equation of hydrostatic equilibrium for the vertical direction is then

$$\frac{1}{\rho}\frac{dp}{dZ} = -\frac{GM_s Z}{(R^2 + Z^2)^{3/2}}, \tag{A1}$$

where R and Z are cylindrical coordinates. Using the adiabatic relation to eliminate the pressure p, we obtain

$$\gamma K \rho^{\gamma - 2} d\rho = -\frac{GM_s Z}{(R^2 + Z^2)^{3/2}}\, dZ . \tag{A2}$$

With the substitution $x = Z^2$, we can integrate this equation to obtain

$$\rho^{\gamma - 1} = \left(\frac{\gamma - 1}{\gamma}\right)\frac{GM_s}{K}\left[\frac{1}{(R^2 + Z^2)^{1/2}} + C\right], \tag{A3}$$

where C is an integration constant. We specify C by defining $\rho(Z = 0) = \rho_0$, yielding

$$\rho(R, Z)^{\gamma - 1} = \rho_0^{\gamma - 1} - \left(\frac{\gamma - 1}{\gamma}\right)\frac{GM_s}{K}\left[\frac{1}{R} - \frac{1}{(R^2 + Z^2)^{1/2}}\right]. \tag{A4}$$

A2. SELF-GRAVITATING THIN DISK

We now derive the approximate vertical equilibrium of a thin ($Z \ll R$), adiabatic disk subject to its own self-gravity as well as that of a central point mass. In this case the equation of vertical hydrostatic equilibrium is

$$\frac{1}{\rho}\frac{dp}{dZ} = -\frac{GM_s Z}{R^3} - 2\pi G\sigma \,, \tag{A5}$$

where σ is the disk surface density, and the term containing σ represents the gravitational attraction from an infinite sheet with uniform surface mass density. Again eliminating the pressure p, we obtain

$$\gamma K \rho^{\gamma-2} d\rho = -\left(\frac{GM_s Z}{R^3} + 2\pi G\sigma\right) dZ \,. \tag{A6}$$

This equation is easily integrable to yield

$$\rho(R, Z)^{\gamma-1} = \rho_0(R)^{\gamma-1} - \left(\frac{\gamma-1}{\gamma}\right)\left\{\left[\frac{2\pi G\sigma(R)}{K}\right]Z + \left(\frac{GM_s}{2KR^3}\right)Z^2\right\} , \tag{A7}$$

where the integration constant has again been specified through the midplane value $\rho(R, Z = 0) = \rho_0(R)$. The second term on the right-hand side arises from the self-gravity of the disk, and the third term from the gravity of the central mass point.

A3. *ANSATZ* DISK

Comparing the above equations (A4) and (A7) suggests a simple form which combines the physics of both configurations. Noting that the second and third terms on the right-hand side of equation (A4) reduce to the third term on the right-hand side of equation (A7) in the limit of a thin disk, we make the *Ansatz* that the vertical equilibrium structure of a fat, adiabatic disk with self-gravity and a central mass is given approximately by

$$\rho(R, Z)^{\gamma-1} = \rho_0(R)^{\gamma-1} - \left(\frac{\gamma-1}{\gamma}\right)\left\{\left[\frac{2\pi G\sigma(R)}{K}\right]Z + \frac{GM_s}{K}\left[\frac{1}{R} - \frac{1}{(R^2+Z^2)^{1/2}}\right]\right\} . \tag{A8}$$

Note that in the limit of negligible disk mass ($\sigma \to 0$), equation (A4) is recovered, while in the limit of a thin disk ($Z \ll R$), equation (A7) is recovered.

A4. RADIAL VARIATION

Specification of the midplane density profile $\rho_0(R)$ is necessary in order to complete the description of the disk. For a disk which is exactly in Keplerian rotation, there can be no radial variation, because the resulting radial pressure gradient will produce non-Keplerian rotation. Clearly realistic disks cannot be exactly Keplerian. Here we examine the relation between a radial pressure gradient and nearly Keplerian rotation.

The radial equation of hydrostatic equilibrium is

$$\frac{1}{\rho}\frac{dp}{dR} = R\Omega^2 - \frac{GM_s R}{(R^2+Z^2)^{3/2}} \,. \tag{A9}$$

We expand the angular velocity Ω in terms of the Keplerian value $\Omega_K^2 = GM_s/R^3$, as $\Omega = \Omega_K + \Omega'$, with $\Omega' \ll \Omega_K$. Eliminating the pressure, we obtain to first-order in Ω

$$K\gamma\rho^{\gamma-2}\frac{d\rho}{dR} = 2R\Omega'\left(\frac{GM_s}{R^3}\right)^{1/2} + \frac{GM_s}{R^2}\left[1 - \left(1 + \frac{Z^2}{R^2}\right)^{-3/2}\right] . \tag{A10}$$

At the midplane ($Z = 0$), we have simply

$$K\gamma\rho^{\gamma-2}\frac{d\rho}{dR} = 2R\Omega'\left(\frac{GM_s}{R^3}\right)^{1/2} . \tag{A11}$$

If we now impose the restriction that $\Omega' \ll \Omega_K$ everywhere in the disk (i.e., that the radial pressure gradient does not dominate centrifugal acceleration anywhere in the disk), then we find

$$\frac{K\gamma\rho^{\gamma-2}}{2}\frac{d\rho}{dR} \ll R\Omega_K^2 \,. \tag{A12}$$

If the density is expressed as a power law $\rho \propto R^{-a}$, then equation (A12) can be satisfied everywhere provided that

$$a = \frac{1}{\gamma - 1} \,, \tag{A13}$$

so that the choice of the adiabatic exponent γ then determines the exponent for the radial density profile.

REFERENCES

Adachi, I., Hayashi, C., & Nakazawa, K. 1976, Prog. Theor. Phys., 56, 1756
Adams, F. C., Emerson, J. P., & Fuller, G. A. 1990, ApJ, 357, 606
Adams, F. C., & Shu, F. H. 1985, ApJ, 296, 655
———. 1986, ApJ, 308, 836
Beckwith, S. V. W., Sargent, A. I., Chini, R. S., & Güsten, R. 1990, AJ, 99, 924
Bodenheimer, P., Yorke, H. W., Różyczka, M., & Tohline, J. E. 1990, ApJ, 355, 651
Boss, A. P. 1984, ApJ, 277, 768
———. 1988, Science, 241, 565
———. 1989, ApJ, 345, 554
———. 1990, in Origin of the Earth, ed. H. E. Newsom & J. H. Jones (New York: Oxford Univ. Press), 3
Boss, A. P., & Black, D. C. 1982, ApJ, 258, 270
Boss, A. P., & Graham, J. A. 1993, Icarus, in press
Boss, A. P., & Myhill, E. A. 1992, ApJS, 83, 311
Boss, A. P., & Yorke, H. W. 1993, ApJ, 411, L99
Cabot, W., Canuto, V. M., Hubickyj, O., & Pollack, J. B. 1987, Icarus, 69, 423
Cassen, P. 1992, Lunar Planet. Sci. Conf., XIII, 207
Cassen, P. M., & Moosman, A. 1981, Icarus, 48, 353
Cassen, P. M., & Summers, A. 1983, Icarus, 53, 26
Goldreich, P., & Ward, W. R. 1973, ApJ, 183, 1051
Hewins, R. H. 1988, in Meteorites and the Early Solar System, ed. J. F. Kerridge & M. S. Matthews (Tucson: Univ. Arizona Press), 660
Hood, L. L., & Horanyi, M. 1991, Icarus, 93, 259
Larimer, J. W., & Wasson, J. T. 1988, in Meteorites and the Early Solar System, ed. J. F. Kerridge & M. S. Matthews (Tucson: Univ. Arizona Press), 394
Lin, D. N. C., & Papaloizou, J. 1980, MNRAS, 191, 37
Lin, D. N. C., & Pringle, J. E. 1990, ApJ, 358, 515
Lissauer, J. J. 1987, Icarus, 69, 249
Morfill, G. E. 1988, Icarus, 75, 371
Mumma, M. J., Weissman, P. R., & Stern, S. A. 1992, in Protostars & Planets III, ed. E. H. Levy, J. I. Lunine, & M. S. Matthews (Tucson: Univ. Arizona Press), 1177
Münch, G. 1960, in Stellar Atmospheres, ed. J. L. Greenstein (Chicago: Univ. Chicago Press), 1
Palme, H., & Boynton, W. V. 1992, in Protostars & Planets III, ed. E. H. Levy, J. I. Lunine, & M. S. Matthews (Tucson: Univ. Arizona Press), 979
Pollack, J. B., McKay, C. P., & Christofferson, B. M. 1985, Icarus, 64, 471
Pringle, J. E. 1981, ARA&A, 19, 137
Ruden, S., & Lin, D. N. C. 1986, ApJ, 308, 883
Ruden, S. P., & Pollack, J. B. 1991, ApJ, 375, 740
Ruzmaikina, T. V., & Maeva, S. V. 1986, Astron. Vestnik, 20, 212
Safronov, V. S., & Ruzmaikina, T. V. 1985, in Protostars & Planets II, ed. D. C. Black & M. S. Matthews (Tucson: Univ. Arizona Press), 959
Schwarzschild, M. 1965, Structure & Evolution of the Stars (New York: Dover), 296
Shu, F. H. 1977, ApJ, 214, 488
———. 1991, The Physics of Astrophysics. I. Radiation (Mill Valley, CA: University Science Books)
Stahler, S. W., Shu, F. H., & Taam, R. E. 1980a, ApJ, 241, 637
———. 1980b, ApJ, 242, 226
Stemwedel, S. W., Yuan, C., & Cassen, P. 1990, ApJ, 351, 206
Stevenson, D. J., & Lunine, J. I. 1988, Icarus, 75, 146
Terebey, S., Shu, F. H., & Cassen, P. 1984, ApJ, 286, 529
Tomley, L., Cassen, P., & Steiman-Cameron, T. 1991, ApJ, 382, 530
Toomre, A. 1964, ApJ, 139, 1217
Tscharnuter, W. M. 1987, A&A, 188, 55
Tscharnuter, W. M., & Winkler, K.-H. 1979, Comput. Phys. Comm., 18, 171
Watanabe, S., Nakagawa, U., & Nakazawa, K. 1990, ApJ, 358, 282
Weidenschilling, S. J. 1977, Ap&SS, 51, 153
Wetherill, G. W. 1990, Ann. Rev. Earth Planet. Sci.,18, 205
Winkler, K.-H., & Newman, M. J. 1980, ApJ, 236, 201
Wood, J. A. 1984, Earth Planet. Sci. Lett., 70, 11
———. 1988, ARE&PS, 16, 53
Wood, J. A., & Morfill, G. E. 1988, in Meteorites and the Early Solar System, ed. J. F. Kerridge & M. S. Matthews (Tucson: Univ. Arizona Press), 329
Yorke, H. W. 1980, A&A, 86, 286